Lithium Storage

DOI: 10.1002/ange.201107885

Reversible Lithium-Ion Storage in Silver-Treated Nanoscale Hollow Porous Silicon Particles**

Dongyun Chen, Xiao Mei, Ge Ji, Meihua Lu, Jianping Xie, Jianmei Lu,* and Jim Yang Lee**

Among rechargeable batteries, lithium-ion chemistry is currently unmatched in terms of energy and power densities.[1–3] The performance of lithium-ion batteries is determined mainly by the choice of anode and cathode materials. Carbon anodes have been ubiquitous in current designs but are limited by a theoretical capacity of 372 mAh g^{-1}.[4,5] There is therefore great interest in the pursuit of high-capacity anode materials. Silicon-based anodes are the most appealing alternative through a combination of high specific capacity (ca. 4140 mAh g^{-1}) and low discharge potentials.[6–12] However, their low electrical conductivity and large volume changes between the charged and discharged states (>300%) are detrimental to cycling stability.[13] A rapid decline in capacity occurs with cycling as a result of the mechanical disintegration of the Si particles and their re-aggregation, which is coupled with a loss of electrical connectivity.

There are two main strategies for improving the electrochemical performance of Si anode materials. The first is to apply a carbon coating to the Si which serves three purposes: to maintain the electrical connectivity between the Si particles, as a soft medium to buffer the stress of volume excursions, and as a barrier against the re-aggregation of Si nanoparticles.[14–20] However, the specific capacity and rate performance of carbon-coated Si anodes are affected by the quality of carbon, which is often not as good as graphite because of the low temperature used for the preparation of the carbon-coating. The use of conductive metal particles (e.g., Ag, Cu) may address such inadequacy and improves cycle stability through conductivity resilience.[21–23]

The second approach exploits the structure-dependent properties of nanosilicon. Recent studies have shown that Si nanoforms, such as Si nanowires and nanotubes, are more resistant to volume changes.[6,24,25] However, the preparation of these Si nanoforms requires substantial retooling of the current fabrication process, making these materials relatively costly and not amenable to quantity production.[26] Hence new designs of Si anodes with the desired combination of functional features have to be supplemented by cost-effective preparation methods. In this context the recent developments on hollow or porous Si nanostructures look quite promising.[21,27] The electrochemical performance of hollow or porous Si anodes is strongly dependent on the free volume in the nanostructure which is used to cushion the volume changes. We hypothesize that Si particles in a smaller size regime (nanoscale, that is, ca. 100 nm) and a well-defined hollow porous structure, for example, a hollow interior and an organized mesoporous shell, can provide a more effective free volume for the uniform distribution of the induced stress and strain, and consequently improve the electrochemical performance. Furthermore if the porosity in the hollow nanoparticle system is created as the intervening space between small primary Si nanoparticles that constitute the shell, the accessibility of the Si host to lithium ions can also benefit from the orderly arrangement and the shorter diffusion path of nanoscale materials.[27,28]

Herein we report a facile approach to fabricate monodisperse hollow porous Si (HPSi) nanoparticles (ca. 120 nm) by the magnesiothermic reduction of hollow porous SiO_2 ($HPSiO_2$) nanoparticles formed by a templating method. This step is followed by Ag coating the nanoparticle for conductivity enhancement. The HPSi anode prepared as such shows several desirable electrochemical features: a high specific reversible capacity (3762 mAh g^{-1}), good cycle stability (over 93% capacity retention after 99 cycles), good rate performance (over 2000 mAh g^{-1} at 4000 mA g^{-1}), surpassing the performance of anode materials based on micron size macroporous Si particles.[21]

As shown in Scheme 1, the fabrication of HPSi nanoparticles is relatively simple and involved two consecutive steps (see Supporting Information). The first step was the preparation of $HPSiO_2$ nanoparticles using polystyrene (PS) nanoparticles (120 nm) as the template and tetraethyl orthosilicate (TEOS) as the Si source and cetyltrimethylammonium bromide (CTAB) as a pore forming sufactant. The reaction was carried out in an ethanol/water mixture (ethanol/

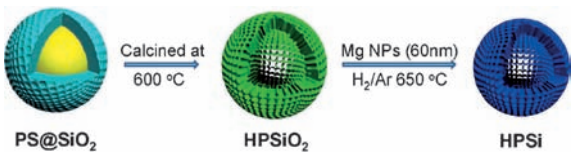

Scheme 1. Preparation of hollow porous Si (HPSi) nanoparticles.

[*] D. Chen, X. Mei, Prof. J. Lu
College of Chemistry
Chemical Engineering and Materials Science
Soochow University, Suzhou, 215123 (China)
E-mail: lujm@suda.edu.cn

G. Ji, M. Lu, Prof. J. Xie, Prof. J. Y. Lee
Department of Chemical & Biomolecular Engineering
Faculty of Engineering, National University of Singapore
10 Kent Ridge Crescent, Singapore, 119260 (Singapore)
E-mail: chexiej@nus.edu.sg
cheleejy@nus.edu.sg

[**] The attachment of D.C. to the National University of Singapore is partially financially supported by the China Scholarship Council (CSC).

Supporting information for this article is available on the WWW under http://dx.doi.org/10.1002/anie.201107885.

water ratio of 2/3 v/v) at room temperature for 12 h, followed by calcination at 600 °C for 6 h to remove the templating PS nanoparticles and CTAB. The second step was the synthesis of HPSi nanoparticles by the magnesiothermic reduction of $HPSiO_2$ nanoparticles.[29] For this step the $HPSiO_2$ nanoparticles were mixed with magnesium nanoparticles (60 nm) and heated at 650 °C for 5 h in 5 vol% H_2 in argon. Acid etching was then used to remove residual magnesium and SiO_2 to leave only the HPSi nanoparticles behind.[29]

A representative TEM image of the $HPSiO_2$ nanoparticles is shown in Figure 1 a. The nanoparticles were spherical, nearly monodisperse, and had an average diameter of approximately 150 nm. The strong contrast between the darker peripheral (ca. 20 nm in thickness) and the lighter central (ca. 110 nm) regions in the TEM image indicates that the nanoparticles had a hollow interior. The HPSi nanoparticles fabricated from the $HPSiO_2$ nanoparticles are shown in Figure 1 b–d. The average size of the HPSi nanoparticles of approximately 120 nm in Figure 1 b represents a approximately 30 nm shrinkage of the $HPSiO_2$ nanoparticles, which can be explained by the reduction in specific volume when SiO_2 was converted into Si. In addition, surface area decreased from 297 $m^2 g^{-1}$ for the $HPSiO_2$ nanoparticles to 112 $m^2 g^{-1}$ for the HPSi nanoparticles (Supporting Information, Figure S1). The surface area decrease is due to changes in particle size and pore structure during magnesiothermic reduction and the subsequent acid treatment. The hollow interior and the porosity in the shell of the HPSi nanoparticles can be seen in the TEM image (Figure 1 b, inset) as a brighter central region (ca. 70 nm) surrounded by a dark discontinuous ring (ca. 25 nm).

High-angle annular dark-field scanning transmission electron microscopy (HAADF-STEM; Figure 1 c) confirmed the hollow interior structure with additional evidence provided by Si intensity line scans. Well-resolved lattice planes can be identified in the high-resolution TEM (HRTEM) image (Figure 1 d) of the nanoparticles. The measured interplanar distance of approximately 0.31 nm corresponds well with the (111) planes of the Si diamond structure. The successful synthesis of phase-pure cubic Si nanoparticles was further corroborated by selected-area electron diffraction (SAED, Figure 1 d, inset) and powder X-ray diffraction (XRD, Figure 2 a, blue line). The diffraction patterns from these measurements could all be indexed to the diamond cubic phase of Si (JCPDS card No. 27-1402).

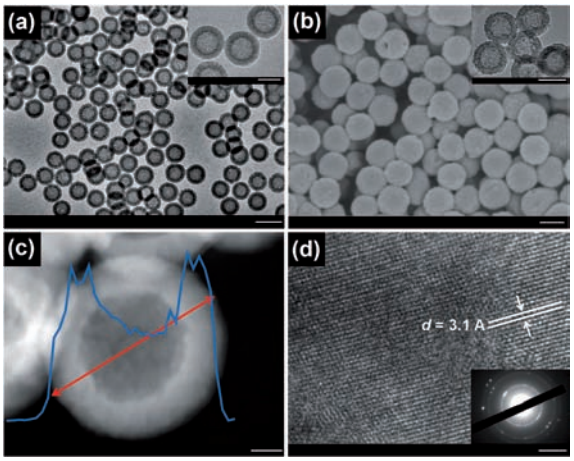

Figure 1. a) TEM (scale bar 200 nm) and high-magnification TEM image (inset, scale bar 100 nm) of $HPSiO_2$ nanoparticles. b) FESEM (scale bar 100 nm), c) STEM (scale bar 20 nm) and Si intensity line scan, and d) HRTEM image (scale bar 5 nm) of HPSi nanoparticles. The inset in (b; scale bar 100 nm) shows a high-magnification TEM image and the inset in (d) shows the SAED pattern of the HPSi nanoparticles.

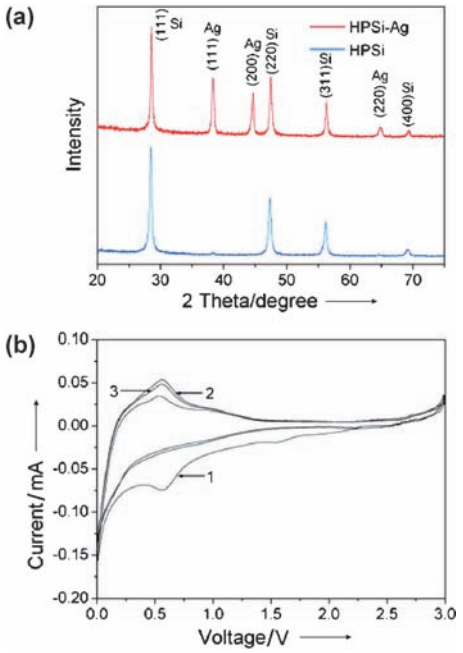

Figure 2. a) XRD patterns of HPSi nanoparticles (blue line) and HPSi-Ag nanocomposite (red line). b) Cyclic voltammograms of HPSi-Ag nanocomposite at a scan rate of 0.1 $mV s^{-1}$ (cycles numbered).

The magnesiothermic-reduced HPSi nanoparticles were treated with Ag nanoparticles (to give HPSi-Ag nanocomposite) to improve their electrical conductivity. XRD measurements were used to analyze the composite structure. Three additional reflections corresponding well with the diffractions of face-centered cubic (fcc) Ag (JCPDS Card No. 4-783) were detected in the HPSi-Ag nanocomposite (Figure 2 a, red line). Elemental mapping by energy-dispersive X-ray spectroscopy (EDS) (Supporting Information, Figure S2) indicated the uniform dispersion of Ag nanoparticles in HPSi nanoparticles. The measured wt% of Ag and Si were 7.7 and 92.3 respectively, which were also confirmed by inductively coupled plasma mass spectrometry (ICP-MS). The Ag nanoparticles within the pores of the HPSi nanoparticles (Supporting Information, Figure S3) electrically connected the Si nanoparticles to the current collector, which should lead to improvements in the electrochemical performance of the HPSi structure. The BET surface area of HPSi-Ag nanocomposite of about 103 $m^2 g^{-1}$ (Supporting Information, Fig-

ure S4) is similar to that of the HPSi nanoparticles, thus suggesting a relatively minor effect of Ag treatment on the nanocomposite surface area. The porosity in the HPSi-Ag shell and the electronic wiring of the Si nanoparticles in the shell shortened the diffusion paths of both lithium ions and electrons. The free volume in the pores and the hollow interior also effectively buffered the volume excursion in lithium ion insertion and extraction reactions in Si (which could amount to 300%).

The electrochemical performance of HPSi-Ag nanocomposite was first evaluated by cyclic voltammetry (CV) in the 0–3.0 V voltage window (Figure 2b). The sharp peak at 0.56 V in the first discharge scan agrees well with the lithiation-induced amorphization of crystalline Si (Li_xSi),[30] although solid–electrolyte interface (SEI) formation may also contribute to it.[31,32] It disappeared from the second cycle onwards indicating the complete amorphization of Si in the first cycle. Two distinct peaks at 0.37 and 0.54 V appeared in the first reverse anodic scan, which could be attributed to the reaction between amorphous Li_xSi and amorphous silicon. Peak current density and integrated area intensity were nearly unchanged in the subsequent discharge and charge cycles, indicating very small capacity losses during cycling. It should be mentioned that Ag can alloy with lithium.[33] However, no redox peaks other than those arising from Si were found in the cyclic voltammogram of the HPSi-Ag nanocomposite (Figure 2b), suggesting that the small amount of Ag nanoparticles (ca. 2 mole%) in the HPSi-Ag nanocomposite served primarily as a conducting additive and contributed negligibly to the measured capacity.

The HPSi-Ag nanocomposite was first cycled at 100 $mA\,g^{-1}$ in the 5 mV to 2.0 V voltage window. The first cycle discharge and charge capacities from Figure 3a were 3762 and 3146 $mAh\,g^{-1}$ respectively. The first cycle coulombic efficiency (CE) of approximately 84% is higher than previously reported values.[21,28] The charge capacity was relatively constant from the second cycle onwards indicating an unusually high stability for a Si-based anode.[10,12,21,26,28] The high reversible capacity and good capacity retention of the HPSi-Ag nanocomposite could be attributed to its unique architecture which combined nanoscale material, conductivity improvement, and free volume creation (a hollow interior and the porosity in the shell) to address the Si deficiencies in battery applications.

For the confirmation of the contributions of free volume and conductivity, the performance of the HPSi-Ag nanocomposite in extended cycling (100 cycles) was compared with the HPSi nanoparticles (no conductivity improvement) and approximately 100 nm commercial Si nanoparticles (no conductivity improvement and no free volume). As shown in Figure 3b, a rapid capacity decline occurred in the commercial Si nanoparticles. The large size of these particles resulted in poor strain relaxation. The uneven distribution of the induced stress caused differential cracking to occur in the particles. The situation improved somewhat in the case of the HPSi nanoparticles (Figure 3b, blue) where a smaller particle size and the presence of free volume were more accommodating to the volume change in charge and discharge reactions. While the active particles might not break down into powder to the same extent, the free volume could also increase the likelihood of electrical disconnection between active Si particles. In the HPSi-Ag nanocomposite (Figure 3b, black), the intervening space between the Si particles was filled with highly conductive Ag nanoparticles (Figure S3) so that the active material could remain electrically connected despite the volume changes. Consequently it had the best

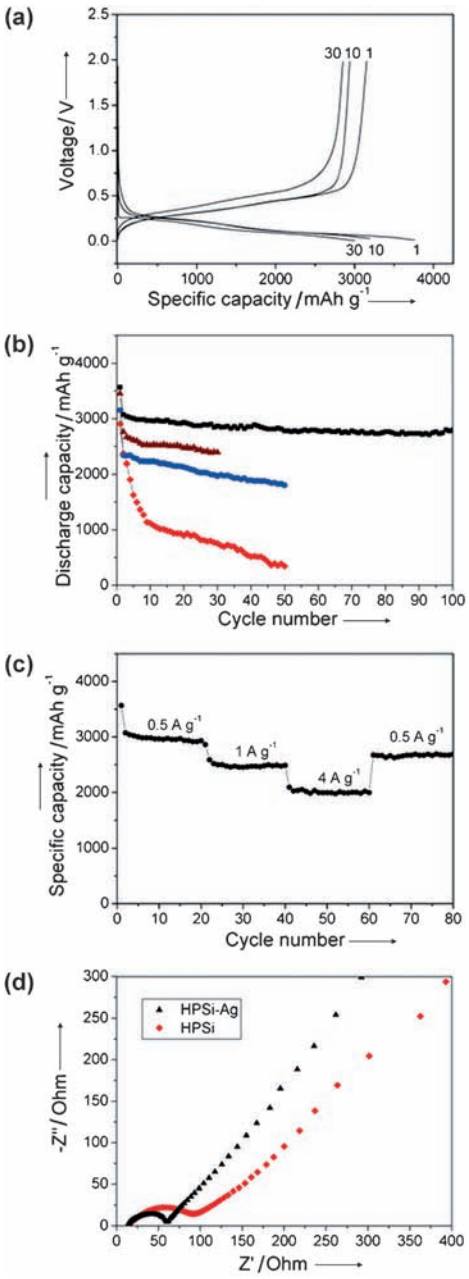

Figure 3. Electrochemical performance of HPSi-Ag nanocomposite electrode: a) galvanostatic charge–discharge profiles in the 5 mV–2 V window (vs. Li/Li^+) for the 1st, 10th, and 30th cycles at 100 $mA\,g^{-1}$; b) discharge capacities of HPSi-Ag nanocomposite (black), HPSi-C nanocomposite (brown), HPSi nanoparticles (blue), and commercial Si nanoparticles (ca. 100 nm, red) at 500 $mA\,g^{-1}$; c) rate performance of HPSi-Ag nanocomposite at different current densities; and d) impedance measurements of HPSi-Ag nanocomposite (black) and HPSi nanoparticles (red).

capacity retention properties. Irreversible capacity losses (ICL) (ca. 16%) were confined only to the first cycle and could be attributed to mainly SEI formation on the Si nanoparticle surface.[34] ICL was higher in the other two electrodes since in addition to SEI formation, there might also be irreversible trapping of the lithium ions through the loss of conductivity in cracking and crumbling of the electrode.[20]

The HPSi nanoparticles were also coated with carbon (HPSi-C nanocomposite) prepared by chemical vapor deposition (CVD) to compare the effectiveness of different conductivity enhancers. The composition was similar to that of the HPSi-Ag nanocomposite except for the coating material. Figure 3b shows that the capacity of the HPSi-C nanocomposite is intermediate between the capacities of HPSi-Ag nanocomposite and HPSi nanoparticles. TEM analysis revealed some partial deconstruction of the HPSi and HPSi-C nanostructures after 30 cycles (Supporting Information, Figure S5a and S5b). This result could explain their lower electrochemical performance than HPSi-Ag for which no structural changes were apparent even after 100 cycles (Figure S5c). The highly conductive small Ag nanoparticles within the pores of the HPSi-Ag nanocomposite (Supporting Information, Figure S3), with their greater rigidity and smaller deformability than carbon, were more able to keep the Si nanoparticles electrically connected and preserved the HPSi architecture during repeated cycling. Hence the conductive Ag nanoparticles were essential in stabilizing the cycling performance of the HPSi-Ag nanocomposite.

The rate performance of HPSi-Ag nanocomposite from 0.5 to 4 $A\,g^{-1}$ was also evaluated in discrete steps. Figure 3c shows very good cycling behavior at these current densities. A specific capacity of over 2000 $mA\,h\,g^{-1}$, or about 70% of the capacity at 0.5 $A\,g^{-1}$, was sustainable at a higher current density of 4 $A\,g^{-1}$. Furthermore, greater than 93% of the capacity at 0.5 $A\,g^{-1}$ was recoverable after cycling at these higher rates. The rate performance of HPSi nanoparticles was also evaluated for comparison. The capacity decrease (Supporting information, Figure S6) when the HPSi nanoparticles were cycled at the high current rate of 4 $A\,g^{-1}$ was more acute. In addition, less than 65% of the capacity at 0.5 $A\,g^{-1}$ was recovered after the high rate cycling as a result of the partial deconstruction of the HPSi nanostructure by high rate cycling. The stability and good rate performance of the HPSi-Ag nanocomposite had much to be credited to the robustness of the nanocomposite microstructure.

The electrochemical impedance spectra (EIS) of HPSi-Ag and HPSi electrodes were also measured to provide further insights. The Nyquist plots in Figure 3d for HPSi-Ag and HPSi electrodes show a straight line in the low frequency region and a depressed semicircle in the high frequency region. The size of the semicircle, which measures the resistance to charge transfer in the electrode,[35] was clearly smaller for the HPSi-Ag electrode. The greater connectivity of the HPSi nanoparticles by the Ag nanoparticles could be the main reason for the reduction in charge-transfer resistance.

In summary, a HPSi nanocomposite with Ag nanoparticles was fabricated by the magnesiothermic reduction of $HPSiO_2$ nanoparticles formed by a templating method. The free volume in the hollow particle interior and the porosity in the shell effectively cushioned the volume changes in Li–Si alloying and de-alloying reactions, and improved the accessibility of the Si host to lithium ions. The ordered construction and the nanoparticle origin of the shell contributed to reducing the diffusion resistance in charge-transfer reactions. The Ag nanoparticles were essential for retaining the electrical connectivity of the Si nanoparticles. Hence high specific reversible capacity (3762 $mA\,h\,g^{-1}$), good cycling stability (over 93% capacity retention) and rate performance (over 2000 $mA\,h\,g^{-1}$ at 4000 $mA\,g^{-1}$) were simultaneously possible for the Ag-treated HPSi nanocomposite. The fabrication process developed herein therefore improves the practicality of using high capacity anode materials with large volume excursions for lithium-ion batteries.

Received: November 9, 2011
Revised: December 22, 2011
Published online: January 27, 2012

Keywords: anode materials · hollow porous nanostructures · lithium storage · silicon · silver

[1] M. Armand, J. M. Tarascon, *Nature* **2008**, *451*, 652.
[2] J. Tollefson, *Nature* **2008**, *456*, 436.
[3] G. Jeong, Y. U. Kim, H. Kim, Y. J. Kim, H. J. Sohn, *Energy Environ. Sci.* **2011**, *4*, 1986.
[4] M. Holzapfel, H. Buqa, L. J. Hardwick, M. Hahn, A. Würsiga, W. Scheifelea, P. Nováka, R. Kötza, C. Veitb, F.-M. Petratb, *Electrochim. Acta* **2006**, *52*, 973.
[5] Y. Matsumura, S. Wang, J. Mondori, *Carbon* **1995**, *33*, 1457.
[6] H. Kim, M. Seo, M. H. Park, J. Cho, *Angew. Chem.* **2010**, *122*, 2192; *Angew. Chem. Int. Ed.* **2010**, *49*, 2146.
[7] H. Kim, B. Han, J. Choo, J. Cho, *Angew. Chem.* **2008**, *120*, 10305; *Angew. Chem. Int. Ed.* **2008**, *47*, 10151.
[8] J. K. Lee, K. B. Smith, C. M. Haynerb, H. H. Kung, *Chem. Commun.* **2010**, *46*, 2025.
[9] L. F. Cui, L. Hu, J. W. Choi, Y. Cui, *ACS Nano* **2010**, *4*, 3671.
[10] P. Gao, Y. Nuli, Y. S. He, J. Wang, A. I. Minett, J. Yang, J. Chen, *Chem. Commun.* **2010**, *46*, 9149.
[11] S. L. Chou, J. Z. Wang, M. Choucair, H. K. Liu, J. A. Stride, S. X. Dou, *Electrochem. Commun.* **2010**, *12*, 303.
[12] Y. Xu, G. Yin, Y. Ma, P. Zuo, X. Cheng, *J. Mater. Chem.* **2010**, *20*, 3216.
[13] C. K. Chan, H. L. Peng, G. Liu, K. Mcilwrath, X. F. Zhang, R. A. Huggins, Y. Cui, *Nat. Nanotechnol.* **2008**, *3*, 31.
[14] N. Dimov, S. Kugino, M. Yoshio, *J. Power Sources* **2004**, *136*, 108.
[15] M. Holzapfel, H. Buqa, W. Scheifele, P. Novak, F. M. Petrat, *Chem. Commun.* **2005**, 1566.
[16] X. W. Lou, C. M. Li, L. A. Archer, *Adv. Mater.* **2009**, *21*, 2536.
[17] I. S. Kim, P. N. Kumta, *J. Power Sources* **2004**, *136*, 145.
[18] H. Y. Lee, S. M. Lee, *Electrochem. Commun.* **2004**, *6*, 465.
[19] C. S. Wang, G. T. Wu, X. B. Zhang, Z. F. Qi, W. Z. Li, *J. Electrochem. Soc.* **1998**, *145*, 2751.
[20] S. H. Ng, J. Wang, D. Wexler, K. Konstantinov, Z. P. Guo, H. K. Liu, *Angew. Chem.* **2006**, *118*, 7050; *Angew. Chem. Int. Ed.* **2006**, *45*, 6896.
[21] Y. Yu, L. Gu, C. Zhu, S. Tsukimoto, P. van Aken, J. Maier, *Adv. Mater.* **2010**, *22*, 2247.
[22] J. W. Kim, J. H. Ryu, K. T. Lee, S. M. Oh, *J. Power Sources* **2005**, *147*, 227.
[23] B. L. He, B. Dong, H. L. Li, *Electrochem. Commun.* **2007**, *9*, 425.

[24] T. Song, J. Xia, J. H. Lee, D. H. Lee, M. S. Kwon, J. M. Choi, J. Wu, S. K. Doo, H. Chang, W. I. Park, D. S. Zang, H. Kim, Y. Huang, K. C. Hwang, J. A. Rogers, U. Paik, *Nano Lett.* **2010**, *10*, 1710.
[25] L. F. Cui, R. Ruffo, C. K. Chan, H. L. Peng, Y. Cui, *Nano Lett.* **2009**, *9*, 491.
[26] C. Du, C. Gao, G. Yin, M. Chen, L. Wang, *Energy Environ. Sci.* **2011**, *4*, 1037.
[27] Y. Yao, M. T. McDowell, I. Ryu, H. Wu, N. Liu, L. Hu, W. D. Nix, Y. Cui, *Nano Lett.* **2011**, *11*, 2949.
[28] X. W. Lou, L. A. Archer, Z. Yang, *Adv. Mater.* **2008**, *20*, 3987.
[29] Z. Bao, M. R. Weatherspoon, S. Shian, Y. Cai, P. D. Graham, S. M. Allan, G. Ahmad, M. B. Dickerson, B. C. Church, Z. Kang, H. W. Abernathy, III, C. J. Summers, M. Liu, K. H. Sandhage, *Nature* **2007**, *446*, 172.
[30] N. Ding, J. Xu, Y. X. Yao, G. Wegner, X. Fang, C. H. Chen, I. Lieberwirth, *Solid State Ionics* **2009**, *180*, 222.
[31] Y. M. Lee, J. Y. Lee, H. T. Shim, J. K. Lee, J. K. Park, *J. Electrochem. Soc.* **2007**, *154*, A515.
[32] M. Green, E. Fielder, B. Scrosati, M. Wachtler, J. S. Moreno, *Electrochem. Solid-State Lett.* **2003**, *6*, A75.
[33] Y. J. Lee, Y. Lee, D. Oh, T. Chen, G. Ceder, A. M. Belcher, *Nano Lett.* **2010**, *10*, 2433.
[34] J. Graetz, C. C. Ahn, R. Yazami, B. Fultz, *Electrochem. Solid-State Lett.* **2003**, *6*, A194.
[35] R. Ruffo, S. S. Hong, C. K. Chan, R. A. Huggins, Y. Cui, *J. Phys. Chem. C* **2009**, *113*, 11390.

